Canadian Conference - Pacific Conference on Earthquake Engineering 2023
Vancouver, British Columbia
June 25th – June 30th, 2023

Refined Deformation Limit States for Circular Reinforced Concrete Bridge Columns

Saif Aldabagh[1*], Faroque Hossain[2] and George M. Shahria Alam [3]

[1]Bridge Engineer, COWI North America, North Vancouver, BC, Canada
[2]PhD Student, Applied Laboratory for Advanced Materials & Structures (ALAMS), School of Engineering, The University of British Columbia, Kelowna, BC, Canada
[3]Professor and Tier-1 Principal's Research Chair in Resilient & Green Infrastructure, School of Engineering, The University of British Columbia, Kelowna, BC, Canada
[*]saif.aldabagh@ubc,ca (Corresponding Author)

ABSTRACT

One hurdle against the widespread implementation of the performance-based design (PBD) for bridges is the lack of consensus among practitioners, researchers, and code committees on engineering demand parameter (EDP) limits defining the onset of various types of damage and their variability. This study seeks to bring consistency to the PBD methodology by establishing refined EDP limits at concrete cover spalling and bar buckling for circular reinforced concrete bridge columns. To this end, a database consisting of 118 previously tested flexure-dominant bridge columns was formulated and analyzed. EDP limit considered at the member level was drift ratio, whereas at the sectional level, EDP limits considered were material strain and curvature ductility. State-of-the-art symbolic regression was adopted to fit the resulting data to mathematical expressions. At the member level, predicted drift ratio limits at the two damage states obtained with the proposed expressions were associated with lower root-mean-square error (RMSE) than those obtained from other similar expressions in the literature. At the sectional level, drift ratios at concrete cover spalling were adequately predicted with compressive strain limits in concrete ranging from 0.004 to 0.007 and a curvature ductility limit of 6.3. More accurate predictions of drift ratios at bar buckling were attained with variable sectional EDP limits, particularly for columns subjected to relatively high axial load. Two expressions predicting tensile strain limit in the rebar and curvature ductility limit at bar buckling were proposed. The ratios of the measured drift ratio at bar buckling to the drift ratio predicted based on the proposed variable tensile strain limit had a mean of 0.99 and a coefficient of variation (COV) of 33%. Corresponding ratios based on the proposed variable curvature ductility limit had a mean of 1.02 and a COV of 31%.

Keywords: Performance-based design, Concrete Columns, Bar buckling, Concrete spalling, Limit States

INTRODUCTION

Fundamental to the PBD methodology are the engineering demand parameter (EDP) limits which quantify the degree of damage and repair efforts. In PBD, to determine whether performance objectives have been achieved, EDP associated with different seismic hazard levels are compared against the EDP limits. For RC bridge columns, typical EDPs quantifying damage include material strains, ductility ratios, drift ratios, and rotations. Prior to the Vision 2000: Performance-Based Seismic Engineering of Buildings [1] report, EDP limits were byproducts of experimental research on bridge columns which primarily focused on component performance and failure under significant cyclic plastic displacement demands. Hose et al. [2] undertook early research efforts to utilize the results from cyclic tests on RC bridge columns where damage states were given secondary consideration to establish EDP limits. Hose et al. [2] introduced a standard evaluation template to correlate EDPs to damage states based on recorded responses and photographs from previously tested bridge components, sub-assemblages, and systems. Kowalsky [3] performed a series of moment-curvature analyses on RC bridge columns to develop dimensionless curvature relationships for two limit states, serviceability and damage control. Based on those relationships, EDPs such as curvature, displacement ductility, drift ratio, and equivalent viscous damping capacities corresponding to the two limit states were established. Berry and Eberhard [4] developed practical models to predict EDPs (concrete compressive strain, plastic rotation, drift ratio, and displacement ductility) at the onset of concrete cover spalling and longitudinal bar buckling as a function of key column properties. Their models were calibrated using PEER Structural Performance Database [5], which contains results of bridge columns tested under cyclic loading between 1973 and 2002. The ratios of the measured drifts at bar buckling to the drifts predicted from the proposed model had a mean of 0.97 and a coefficient of variation of 24% for circular bridge columns [5]. Lehman and Moehle [6] executed one of the first experimental research programs designed specifically to study damage progression in well-confined circular RC bridge columns. Five columns with varying longitudinal reinforcement ratios and aspect ratios were tested under reversed cyclic loading where various EDPs corresponding to concrete cover spalling, concrete core crushing, and longitudinal bar buckling were reported. While a limited number of specimens were tested by Lehman and Moehle [6], their work laid the foundation for experimental programs primarily focused on the quantification of damage states. Goodnight et al. [7] executed an experimental program similar to that of Lehman and Moehle [6] but considered a wider test matrix and a more advanced strain measurement technique. Test variables included lateral displacement history, axial-load ratio, longitudinal steel reinforcement ratio, aspect ratio, and transverse steel detailing. Based on the reported data, recommendations were made on material strain and drift limits at longitudinal rebar first yield, concrete crushing, yielding of confinement steel, and longitudinal bar buckling. These studies, among others, have made significant contributions to damage quantification in terms of EDPs for RC bridge columns. There is still, however, a noticeable inconsistency in EDP limits specified in literature and guidelines [8, 9]. The inconsistency in EDP limits specified by different researchers, agencies, and design codes at concrete cover spalling and bar buckling is demonstrated in subsequent sections of this study. According to the NCHRP Synthesis 440 [9] bringing consistency to EDP limits for RC bridge columns is a key step forward towards nationwide realization of the PBD methodology.

The present study explores the feasibility of establishing refined uniform EDP limits at concrete cover spalling and longitudinal bar buckling for RC bridge columns. Concrete cover spalling is the first damage state in RC bridge columns signaling the need for costly and time-consuming repair, hence may lead to short-term loss of function [2]. Bar buckling is the first damage state leading to loss of strength in RC bridge columns [10]. At this level of damage, the typical repair strategy is partial or complete replacement of the component or structure. Because of their significant socioeconomic implications, concrete cover spalling and bar buckling damage states are the focus of this study. Similar to the study by Berry and Eberhard [4], EDP limits in this study were based on results of previous cyclic tests on RC bridge columns. The present study, however, differs from that of Berry and Eberhard [4] in key three aspects. First, in this study, EDP limits are based on a larger database of previously tested RC bridge columns. Second, in Berry and Eberhard [4], local responses were determined using simple plastic hinge analysis, whereas in this study, they were determined using fiber-based analysis incorporating state-of-the-art gradient inelastic force-based element formulation [11]. Third, mathematical expressions were fitted to the data in this study using machine learning-based symbolic regression rather than traditional regression [4]. The proposed EDP limits were compared against those found in literature, and design codes and guidelines.

EXPERIMENTAL DATABASE

This study assembled an experimental database of 118 RC bridge columns tested under quasi-static cyclic loading. The database included only circular columns with spiral or circular hoops reinforcement. The assembled database contained columns tested from 1973 onwards. The PEER Structural Performance Database [5] was the primary source for tests before 2003. Extensive review of experimental studies after 2003 resulted in adding 68 columns to the database. Details of columns in the database as well as experimentally reported drift ratios at concrete cover spalling (Δ_{sp}/L) and bar buckling (Δ_{bb}/L) are provided as supplemental data (Table S1). It should be noted that drift ratios corresponding to the two damage states were not reported for all columns in the database. Drift ratios at concrete cover spalling were reported for 101 columns, whereas drift ratios at bar buckling were reported for 103 columns. All of the columns in the database were subjected to standard loading histories consisting of repeated cycles of step-wise increasing deformation amplitudes. In addition, all of the columns experienced flexural failure where damage typically progresses in this order: concrete cracking, longitudinal bar yielding, concrete cover spalling, concrete core crushing, longitudinal bar buckling, spiral fracture, and longitudinal bar fracture [10]. Table 1 provides a statistical summary of key column properties in the database. In Table 1, L is the distance from the column base to the point of contraflexure; D is the column diameter; L/D is the column aspect ratio (sometimes referred to as moment–shear span ratio); f_y is the yield strength of longitudinal reinforcement; f_{yh} is the yield strength of transverse reinforcement; f_c' is the concrete compressive strength; d_b is the diameter of longitudinal rebar diameter; ρ_l is the longitudinal reinforcement ratio; ρ_s is the spiral reinforcement ratio; s/d_b is the ratio of hoop spacing (s) to d_b; and $P/f_c'A_g$ is the axial load ratio which is the ratio of applied vertical load (P) to the product of f_c' and gross cross-sectional area (A_g).

Table 1. Statistical Summary of Key Column Properties in the Database.

Statistic	L (mm)	D (mm)	L/D	f_y (MPa)	f_{yh} (MPa)	f_c' (MPa)	d_{bl} (mm)	ρ_l	ρ_s	s/d_b	$P/f_c'A_g$
Min.	250	750	2.0	294	207	22.4	7.0	0.01	0.001	0.83	0.01
Max.	1520	9140	10.0	565	1000	90.0	43.0	0.04	0.038	12.5	0.70
Median	457	2000	4.0	444	431	32.5	18.4	0.02	0.009	3.5	0.10
Mean	510	2328	4.6	424	428	34.1	17.6	0.02	0.009	4.2	0.20
COV	0.41	0.53	0.36	0.13	0.22	0.33	0.28	0.35	0.56	0.64	0.79

NUMERICAL MODEL DESCRIPTION AND VALIDATION

Element and section discretization of a bridge column based on the adopted modeling strategy is depicted in Fig. 1. As seen in Fig. 1 (a) the bridge column consists of two elements: the first is the GI FB element and the second is a zero-length (ZL) element. According to Salehi et al. [11], to ensure objectivity in the response, the number of integration points (N) within the GI FB element needs to be determined such that the following condition is satisfied:

$$\mathrm{N} \geq \frac{1.5L}{l_c} + 1 \tag{1}$$

where l_c is the characteristic length. l_c can be taken equal to the potential plastic hinge length, L_p (Sideris and Salehi 2016). In this study, L_p was determined following the equation proposed by Priestley et al. [12]:

$$L_p = 0.08L + 0.022 f_y d_b \geq 0.044 f_y d_b \tag{2}$$

Where f_y is the yield strength of longitudinal reinforcement in MPa. Bridge column section is constituted of three types of materials, namely, unconfined concrete, confined concrete, and steel reinforcement, as shown in Fig. 1(b). The stress-strain responses of these materials were simulated using OpenSees *Concrete01* [13], *Concrete04* [14], and *Steel02* [15], respectively. The properties of the confined concrete were determined based on the theoretical stress-strain model proposed by Mander et al. [16] for confined concrete. *Concrete01* and *Concrete04* models are characterized by degraded linear unloading and reloading stiffness under compression according to the work of Karsan-Jirsa [17]. To account for strain penetration effects, the hysteretic model developed by Zhao and Sritharan [18] (known as *BondSP01* in OpenSees) was integrated into the analysis using the zero-length section element shown in Fig. 1. The section of the zero-length element is identical to that of the beam-column element except for the material model assigned to the steel fibers. Instead of the *Steel02* material model, the *BondSP01* model is assigned to the steel fibers in the section of the zero-length element. The *BondSP01* material model represents the bar slip for a given bar stress and includes the following parameters: yield strength of the reinforcement steel (f_y), rebar slip at member interface under yield stress (s_y), ultimate strength of the reinforcement steel (f_u), rebar slip at the loaded end at the bar fracture strength (s_u), initial hardening ratio in the monotonic slip versus bar stress response (*b)*, pinching factor for the cyclic slip versus bar response (*R*). Expressions to compute s_y and s_u; and recommended values for b and R can be found in Zhao and Sritharan (2007). The hysteretic rules of Bond SP01 model were established based on the available test data and observed responses of concrete members under cyclic loading. A detailed description of these rules can be found in Zhao and Sritharan (2007). The effect of shear deformations was not considered in the analysis because all of the selected bridge columns in the database were characterized by flexure-dominated behavior. According to Lehman and Moehle [6], the contribution of shearing deformations to the responses of flexure-dominant bridge columns under cyclic loading is negligible.

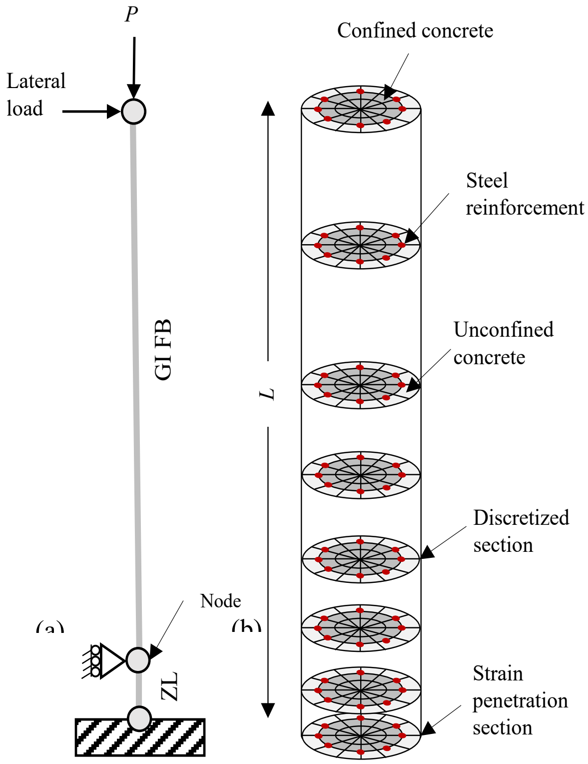

Figure 1. (a) Element, and (b) section discretization of the bridge column.

To validate the numerical model, its predictions were compared against experimentally measured responses at both global/member and local/sectional levels. Test 9, Test 19, and Test 24 from the experimental program by Goodnight et al. [7], which corresponds to Columns 63, 68, and 73, respectively, in the database, were selected for numerical model validation purposes. While these columns vary in their geometry, martial properties, and reinforcement details, they belong to the same experimental program by Goodnight et al. [7]. The reason for limiting the numerical validation specimens to those tested by Goodnight et al. [7] is the high-fidelity reported strain data which were obtained through the use of an optical 3D position measurement system. Details of the material models used to construct the numerical models of the three columns are presented in Tables S2 to S5 (see supplemental data). Fig. 2 provides a comparison between experimentally measured and numerically predicted responses for Test 9, Test 19, and Test 24 at global and local levels. At the global level, measured and predicted force-displacement hysteresis were compared. At the local level, predicted curvature and extreme rebar axial tensile strain distributions were compared against those measured by Goodnight et al. [7] across a wide range of drift ratios. As evident in Fig. 2, the measured responses at local and global levels were predicted fairly well by the numerical model. The average errors between predicted and maximum measured strains over the considered ranges of drift ratios were 9.8%, 6.6%, and 12.2% for Test 9, Test 19, and Test 26, respectively. In addition, the average errors between predicted and maximum measured curvatures over the considered ranges of drift ratios were 8.1%, 4.9%, and 9.5% for Test 9, Test 19, and Test 26, respectively. With percentage error of predictions being generally below 10%, the numerical model accuracy was deemed acceptable for the intended analysis.

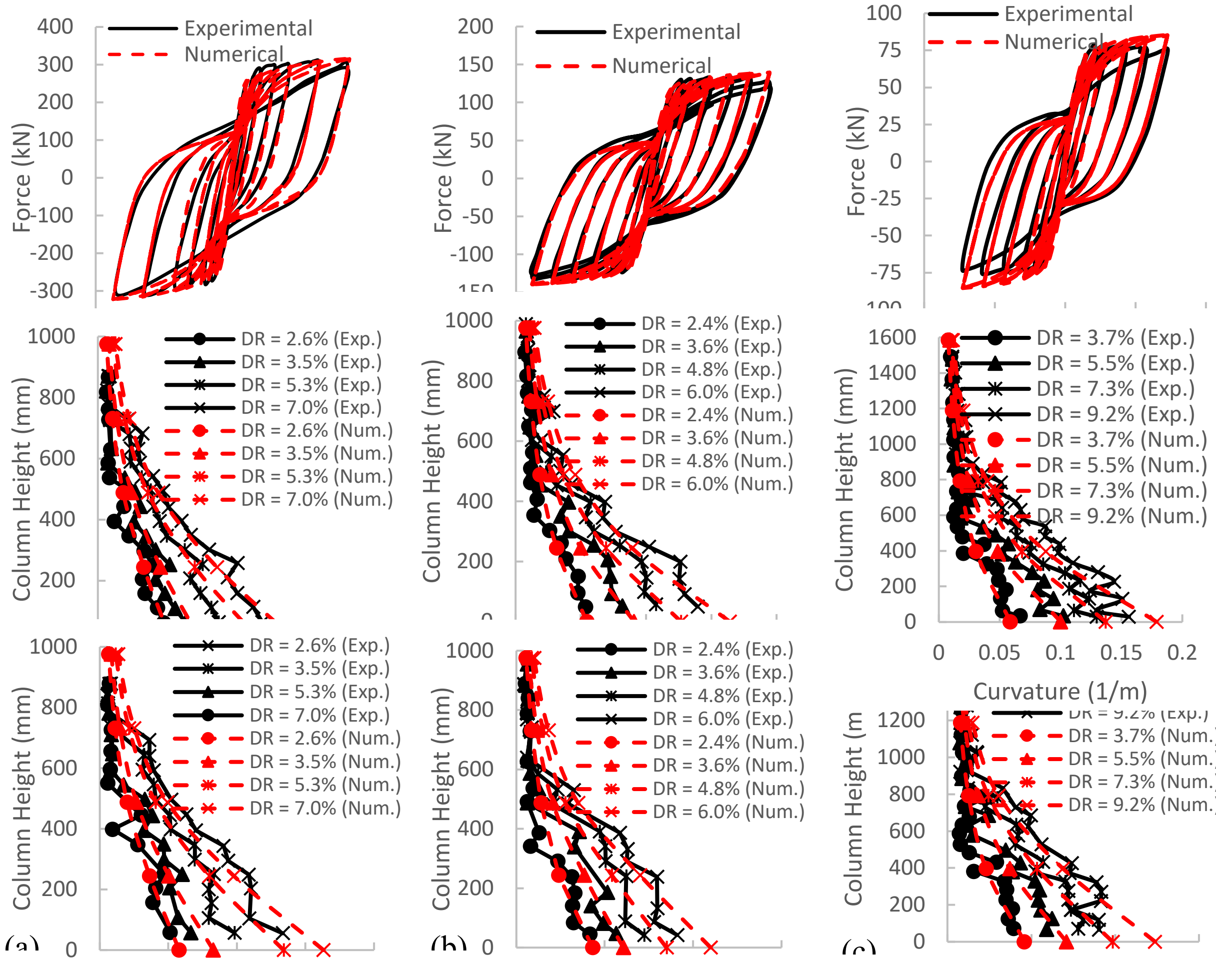

Figure 2. Comparisons between predicted and measured (Goodnight et al. 2015) responses for (a) Test 9; (b) Test 19; and (c) Test 24 (DR = drift ratio).

DRIFT RATIO LIMIT STATES

The first EDP with which the onset of concrete cover spalling and bar buckling was correlated was the drift ratio. Drift ratio has the virtue of ease of interpretation and computation, hence is one of the most attractive EDP for the PBD methodology. A number of expressions predicting drift ratios at concrete cover spalling and bar buckling can be found in the literature. These are presented and considered herein for comparison purposes. Berry and Eberhard [4] combined plastic-hinge analysis with the approximations of yield displacement, plastic curvature, and plastic-hinge length to establish functions predicting drift ratios at concrete cover spalling and bar buckling for circular RC bridge columns. Constants of those functions were calibrated using observations of concrete cover spalling and bar buckling from cyclic tests of 40 and 42 bridge columns, respectively. Berry and Eberhard [4] proposed a three-variable function to predict drift ratio at concrete cover spalling, Δ_{sp}/L, in percent, which takes the following form:

$$\frac{\Delta_{sp}}{L} = 0.007(1 + 2.654\left(\frac{L}{D}\right)^{0.429})\,(1 - 1.229\left(\frac{P}{f_c'A_g}\right)^{0.720})(1 + (151.934\left(\rho_l\frac{f_y}{f_c'}\right)^{0.618}) \quad (3)$$

Berry and Eberhard (2003) also proposed a function to predict drift ratio at bar buckling, Δ_{bb}/L, in percent for circular bridge columns, which takes the following form:

$$\frac{\Delta_{bb}}{L} = 3.25(1 + 150\frac{\rho_s f_{yh}}{f_c'}\frac{d_{bl}}{D})(1 - \frac{P}{f_c'A_g})(1 + \frac{L}{10D}) \quad (4)$$

Goodnight et al. [7] proposed an alternative function to predict Δ_{bb}/L (in percent) based on a larger data set consisting of columns tested by Goodnight et al. [19] and those used in Berry and Eberhard [4] as follows:

$$\frac{\Delta_{bb}}{L} = 0.9 - 3.13\frac{P}{f_c' A_g} + 142000\rho_s\frac{f_{yh}}{E_s} + 0.45\frac{L}{D} \tag{5}$$

where E_s is the modulus of elasticity of the transverse reinforcement. Similar functions were proposed by Aldabagh et al. [20] but based on data obtained from numerical analysis. In Aldabagh et al. [20], an ensemble of hypothetical RC bridge columns having unique combinations of key columns properties was generated using Monte Carlo Simulations and analyzed under monotonic static pushover load where drift ratio limit states at concrete cover spalling and bar buckling were identified by monitoring material strains at sections of maximum moment. Concrete cover spalling was detected when compressive strains in cover concrete reached 0.006, whereas bar buckling was detected when tensile strains in longitudinal rebars reached 0.05. The functions proposed by Aldabagh et al. [20] to predict drift ratios at concrete cover spalling and bar buckling are given in Eqs. (6) and (7), respectively.

$$\frac{\Delta_{sp}}{L} = \frac{79}{10000} + \frac{309}{100000}\frac{L}{D} - \frac{219}{5000}\frac{P}{f_c' A_g} \tag{6}$$

$$\frac{\Delta_{bb}}{L} = \frac{19}{500} + \rho_s + \frac{753}{100000}\frac{L}{D} - \frac{517}{1000000}f_c' - \frac{123}{2500}\frac{P}{f_c' A_g} \tag{7}$$

where f_c' is concrete compressive strength in MPa. According to Aldabagh et al. (2021), Eq (6) had comparable accuracy to that of Eq. (3) in predicting drift ratio at concrete cover spalling, whereas Eq. (7) had higher accuracy than Eqs. (4) and (5) in predicting drift ratio at bar buckling. In this study, alternative functions to predict drift ratios at the two damage states were developed. This was achieved by fitting the reported drift ratio limit states for the columns in the database through an unconventional yet powerful type of regression, the symbolic regression. To limit the complexity of the functions obtained from the symbolic regression, the following constraints were imposed on the algorithm: (1) only up to three-level interaction between column properties was permitted; and (2) model building blocks were limited to constant, addition, subtraction, multiplication, and division. Symbolic regression fitted models to drift ratio data at bar buckling and concrete cover spalling are given in Eqs. (8) and (9), respectively.

$$\frac{\Delta_{sp}}{L} = 0.0198 + 0.00162\frac{L}{D} - 0.0000701f_c' - 0.0238\frac{P}{f_c' A_g} \tag{8}$$

$$\frac{\Delta_{bb}}{L} = 2.96\rho_s + 0.0000607f_{yh} + 0.000479(\frac{L}{D})^2 - 429\frac{P}{f_c' A_g}\rho_s \tag{9}$$

where f_c' and f_{yh} are in MPa. Among the column properties, L/D, f_c', and $P/f_c'\ A_g$ were found to have significant contribution to the drift ratio at concrete cover spalling, whereas L/D, ρ_s, f_{yh}, and $P/f_c'\ A_g$ were found to have significant contribution to drift ratio at bar buckling based on the regression analysis, as seen in Eqs. (8) and (9). Parameters and trends in Eqs. (8) and (9) are in conformity with similar expressions and experimental observations found in the literature. Eqs. (8) and (9) indicate that the increase in L/D increases Δ_{sp}/L and Δ_{bb}/L, respectively. This trend is also observed in Eqs. (3)-(7) and has been reported experimentally by others [6, 7]. On the contrary to L/D, Eqs. (8) and (9) show that the increase in $P/f_c'\ A_g$ decreases Δ_{sp}/L and Δ_{bb}/L, respectively. This is expected since higher axial load ratios are associated with higher compressive strains which accelerate the onset of the concrete cover spalling and bar buckling. Moreover, Eq. 8 indicates a negative correlation between Δ_{sp}/L and f_c'. While such correlation is absent in Eqs. (3) and (6), evidence from experiments suggesting that higher strength concrete crushes at lower compressive strains exist (Moehle 2015). This indicates that concrete bridge columns with higher concrete compressive strength are more susceptible to concrete cover spalling at lower drift ratios. On the other hand, similar to Eqs. (4) and (5), Δ_{bb}/L is positively correlated with f_{yh} in Eq. (9). ρ_s appears in Eq. (9) as an individual parameter and as part of an interaction with $P/f_c'\ A_g$. Δ_{bb}/L is positively correlated with the individual ρ_s because the higher ρ_s provides greater confinement against bar buckling, hence increases the drift ratios at bar buckling for bridge columns. The interaction between ρ_s and $P/f_c'\ A_g$ indicates that the decrease in Δ_{bb}/L because of the increase in $P/f_c'\ A_g$ is more pronounced at higher ρ_s. For example, specimens 101 and 102 had ρ_s of 0.011 and were subjected to axial loads of $0.1f_c'\ A_g$ and $0.2f_c'\ A_g$, respectively. Because of the increase in $P/f_c'\ A_g$, specimen 102 is characterized by lower Δ_{bb}/L than specimen 101 by 19.7%. Specimens 104 and 105, on the other hand, had ρ_s of 0.008 and were subjected to axial loads of $0.1f_c'\ A_g$ and $0.2f_c'\ A_g$, respectively. Because of the increase in $P/f_c'\ A_g$, specimen 105 is characterized by lower Δ_{bb}/L than specimen 104 by 3.9%. The previous observations demonstrate that there are no anomalies in Eqs. (8) and (9).

Table 2. Summary of the Statistics of $\Delta_{Meas.}/\Delta_{Pred.}$ and RMSE.

Statistic	Concrete cover spalling			Bar buckling			
	Eq. 3	Eq. 6	Eq. 8	Eq. 4	Eq. 5	Eq. 7	Eq. 9
Min.	0.46	0.70	0.47	0.43	0.66	0.72	0.51
Max.	2.68	2.13	1.69	1.49	2.08	1.87	1.82
Mean	1.11	1.23	1.00	0.86	1.13	1.08	1.00
COV	0.39	0.31	0.31	0.27	0.25	0.24	0.24
RMSE	0.007	0.008	0.006	0.002	0.002	0.003	0.001

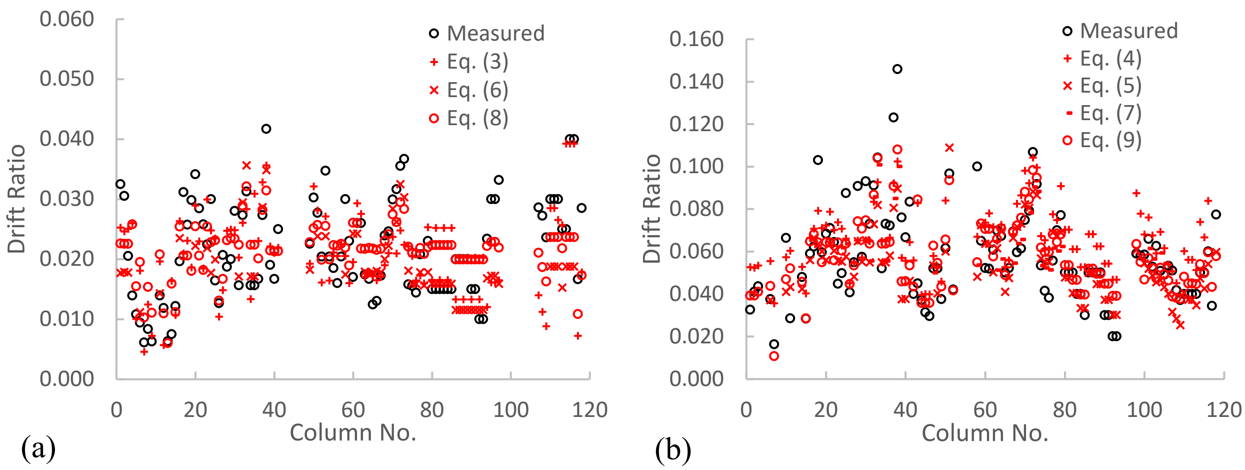

Figure 3. Comparisons between measured and predicted drift ratios at: (a) concrete cover spalling; and (b) bar buckling.

MATERIAL STRAIN LIMIT STATES

The previously described and validated numerical model was used to analyze the bridge columns in the database under reversed cyclic loading where the reported drift ratios at concrete cover spalling and bar buckling are translated into a sectional EDP, material strain, at the section of the maximum moment. Specifically, for concrete cover spalling, computed material strains were at the extreme compression fiber of the cross-sections, ε_c, whereas for bar buckling, they were tensile strains in the extreme longitudinal bars, ε_t. Table S6, which is part of the supplemental data, presents computed material strains for all the columns in the database. For clarity, in subsequent sections of this study, material strains in Table S6 are referred to as *computed material strains* whereas those obtained from existing or proposed expressions are referred to as *predicted material strains*.

Concrete cover spalling

A considerable spread in experimentally reported ε_c at concrete cover spalling for concrete bridge columns exists in the literature. ε_c reported by Berry and Eberhard [4] ranged from 0.002 to 0.018 with a mean of 0.008 and a standard deviation of 0.0045. In the cyclic tests by Lehman et al. [10], concrete cover spalling occurred over a wide range of ε_c (0.0039 to 0.011) with a mean of 0.066 and a standard deviation of 0.022. ε_c at concrete cover spalling ranged from 0.0026 to 0.0085 for concrete bridge columns tested by Goodnight et al. [7] under revered cyclic loading. The considerable spread in reported ε_c in literature has led to variability in the recommended strain limits defining concrete cover spalling, particularly for PBD applications. The computed ε_c for the bridge columns in the database ranged from 0.0027 to 0.023 with a mean of 0.009 and a standard deviation of 0.0055. Symbolic regression analysis was first performed to evaluate the feasibility of fitting the computed ε_c data (Table S6) to a mathematical expression. The resulting equation is as follows:

$$\varepsilon_c = 0.0172 - 0.000174 d_b - 0.000186 f_c' \tag{10}$$

where d_b is the longitudinal bar diameter in mm and f_c' is the concrete compressive strength in MPa. According to Eq. (10), as the longitudinal bar size and concrete compressive strength in bridge columns increase, concrete cover spalling becomes more susceptible to spalling at lower compressive strains. These correlations, however, were regarded as weak correlations because of the low square of correlation coefficient associated with the predictions of Eq. (10), which was equal to 0.3. In addition, the RMSE of the predictions of Eq. (10) was equal to 0.005. The poor correlation between the computed ε_c and predicted ε_c is evident in Fig. 4, where the two are contrasted. As an alternative to Eq. (10), ε_c limit identifying the onset of concrete cover spalling can be established as a constant value. A constant ε_c limit of 0.0067 was found to minimize the RMSE between computed and predicted ε_c at concrete cover spalling to 0.006. The RMSE associated with $\varepsilon_c = 0.006$ is marginally lower than that of Eq. (10), indicating that the added complexity of adopting Eq. (10) to predict ε_c at concrete cover spalling is unjustified. Eq. (10)'s predictions are therefore excluded from subsequent analysis. Horizontal lines in Fig. 4 represent ε_c limit of 0.0067 as well as those recommended by others. The relatively high RMSE associated with ε_c limits at concrete cover spalling irrespective of their value is primarily due to the considerable scatter in computed ε_c, which is evident in Fig. 4. Fig. 5 compares measured and predicted (based on different ε_c limits) drift ratios at concrete cover spalling. Statistics of $\Delta_{Meas.}/\Delta_{Pred.}$ (based on different ε_c limits at concrete cover spalling) and RMSE are summarized in Table 3. As seen in Table 3, varying the ε_c limit had little to no influence on the COV of $\Delta_{Meas.}/\Delta_{Pred.}$ at concrete cover spalling. In addition, the lowest RMSE was associated with ε_c limits of 0.0067 and 0.007. Differences, however, between RMSEs associated with all ε_c limits except that equal to 0.004 appear to be marginal.

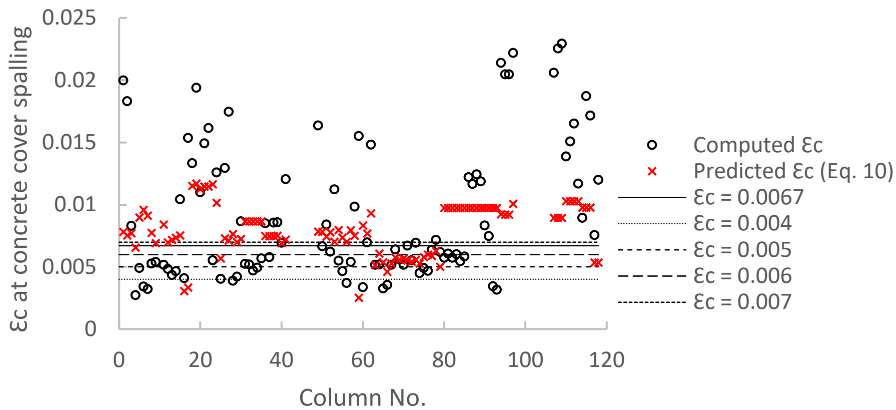

Figure 4. Comparisons between computed and predicted ε_c at concrete cover spalling.

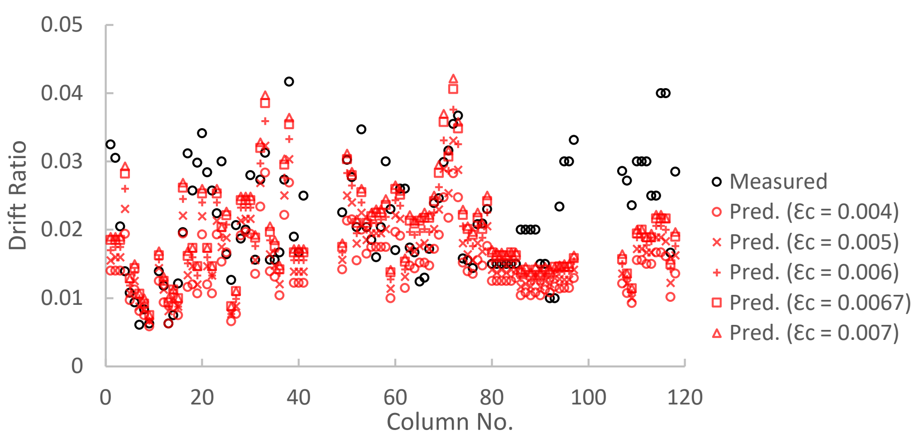

Figure 5. Comparison between experimentally measured and predicted (based on different ε_c limit) drift ratios at concrete cover spalling.

Table 3. Summary of the Statistics of $\Delta_{Meas.}/\ \Delta_{Pred.}$ (Based on Different ε_c Limits at Concrete Cover Spalling) and RMSE.

Statistic	ε_c limits at concrete cover spalling				
	0.004	0.005	0.006	0.0067	0.007
Min.	0.72	0.60	0.54	0.49	0.48
Max.	2.79	2.48	2.24	2.10	2.06
Mean	1.53	1.34	1.23	1.15	1.12
COV	0.35	0.36	0.36	0.36	0.37
RMSE	0.010	0.008	0.008	0.007	0.007

Longitudinal bar buckling

Several recommendations have been made in the literature on ε_t limit at bar buckling in bridge columns. Among the first of such recommendations was that of Kowalsky [3] which suggests that the onset of bar buckling can be correlated with an ε_t limit of 0.06. Goodnight et al. [7] tested 30 large scale reinforced concrete bridge columns and recorded ε_t at bar buckling. ε_t reported by Goodnight et al. [7] ranged from 0.024 to 0.059 with a standard deviation of 0.009. Based on the reported data, Goodnight et al. [7] proposed an expression to predict ε_t at bar buckling, which takes the following form:

$$\varepsilon_t = 0.03 + 700\rho_s \frac{f_{yh}}{E_s} - 0.1\frac{P}{f_c' A_g} \tag{11}$$

The CSA S6 [21] specifics $\varepsilon_t = 0.05$ as the strain limit corresponding to the onset of bar buckling. In this study, computed ε_t for the columns in the database ranged from 0.01 to 0.1 with a standard deviation of 0.021. It should be noted that the effect of subjectivity in damage observation is more pronounced in this study than Goodnight et al. [7] where data were based on a single experimental program. This justifies the wider ranges and higher standard deviation of computed bar tensile strains (ε_t) at bar buckling in this study when compared to those reported by Goodnight et al. (2016). Here, using symbolic regression, the space of mathematical expressions was searched to find the model that best fit the data of computed ε_t at bar buckling. The resulting expression is:

$$\varepsilon_t = 0.0645 + 1.59\rho_s - 0.00163\frac{s}{d_b} - 0.118\frac{P}{f_c' A_g} \tag{12}$$

Fig. 6 provides a comparison between computed ε_t and ε_t predicted with Eqs. (11) and (12). RMSE of the predictions of Eq. (12) is 0.015 which was about half of that of Eq (11)'s predictions. Note that Eq. (11) was applied to only 57 columns in the database not to violate its range constraint. Eq. 11 by Goodnight et al. [7] was not applicable to bridge columns with ρ_{eff} less than 0.05 or subjected to axial load exceeding $0.3f_c' A_g$.This explains the absence of Eq. (11)'s predictions for many columns in Fig. 6. The feasibility of defining ε_t as a constant value was also explored herein. A constant ε_t of 0.056 was found to minimize the RMSE when compared to the computed ε_t in the database. Horizontal lines corresponding to constant ε_t limits of 0.05, 0.056, and 0.06 are overlaid on computed ε_t in Fig. 6.

To assess the accuracy of the constants (0.05, 0.056, and 0.06) as well as the variable (Eqs. 11 and 12) ε_t limits in predicting drift ratio at bar buckling, correspondent drift ratios were determined using the numerical model and compared against measured Δ_{bb}/L for the columns in the database. Fig. 7 compares predicted drift ratios based on various ε_t limits with experimentally measured drift ratios at bar buckling. Statistics of $\Delta_{\text{Meas.}}/\ \Delta_{\text{Pred.}}$ (based on ε_t limits) and RMSE are given in Table 4. For variable ε_t limits at bar buckling, ratios of $\Delta_{\text{Meas.}}$ to $\Delta_{\text{Pred.}}$ based on Eq. (12) were associated with lower RMSE but higher COV than those based on Eq. 11. The higher COV is due to the significantly wider range of applicability of Eq. 12 than Eq. 11. ε_t limits based on Eq. 12 yielded predictions for all bridge columns in the database with reported Δ_{bb}/L (i.e., 103 columns), whereas ε_t limits based on Eq. 11 yielded predictions to only 57 columns. Referring to Table 4, varying the constant ε_t limits had little to no influence on the COV of $\Delta_{\text{Meas.}}/\ \Delta_{\text{Pred.}}$ and RMSE of predicted drift ratios at bar buckling. COV of $\Delta_{\text{Meas.}}/\ \Delta_{\text{Pred.}}$ and RMSE of predicted drift ratios based on constant ε_t limits were higher than those based on variable ε_t limits at bar buckling (see Table 4). This is primarily because constants ε_t limits fail to account for the effect of the axial load ratio, hence often leads to an overestimation of the drift ratios at bar buckling for bridge columns subjected to relatively high axial loads.

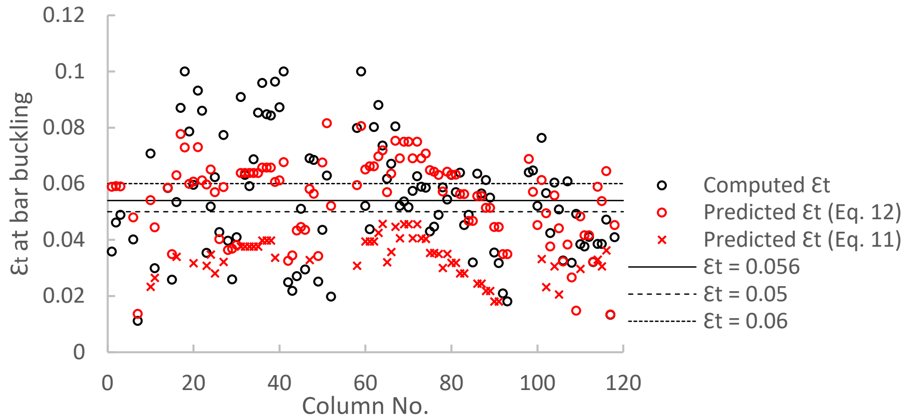

Figure 6. Comparison between computed and predicted ε_t at bar buckling.

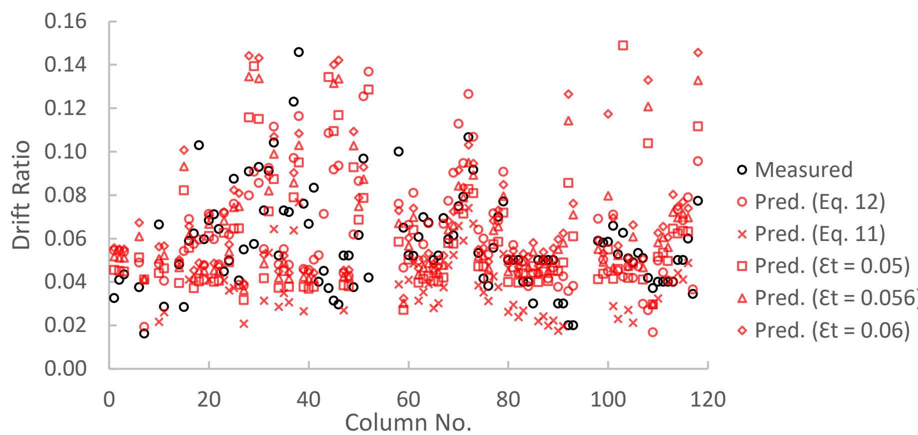

Figure 7. Comparison between experimentally measured and predicted (based on different ε_t limits) drift ratios at bar buckling.

Table 4. Summary of the Statistics of $\Delta_{Meas.}/\ \Delta_{Pred.}$ (Based on Different ε_t Limits at Bar Buckling) and RMSE.

Statistic	ε_t limits at bar buckling				
	Eq. (12)	Eq. (11)	$\varepsilon_t = 0.05$	$\varepsilon_t = 0.056$	$\varepsilon_t = 0.06$
Min.	0.31	1.07	0.23	0.17	0.16
Max.	2.21	3.08	2.56	2.28	2.11
Mean	0.99	1.76	1.11	1.01	0.93
COV	0.33	0.28	0.43	0.41	0.42
RMSE	0.022	0.029	0.031	0.030	0.033

CONCLUSIONS

One hurdle that must be overcome to promulgate the PBD approach is consensus among practitioners, researchers, and code committees on EDP limits at various damage states and their reliability. Establishing consistent EDP limits is, therefore, a significant step forward towards effective, widespread implementation of PBD of bridges. In this study, to develop refined EDP limits identifying the onset of concrete cover spalling and bar buckling in bridge columns, an experimental database of 118 spirally-confined circular columns tested under quasi-static cyclic loading was formulated and analyzed. A validated numerical model employing a new gradient inelastic force-based element formulation was used to translate reported drifts to sectional EDPs, material strains and curvature ductility, at the two damage states. Symbolic regression incorporating state-of-the-art machine learning-based algorithm was used to search for best-fit mathematical expressions. Drift ratio predictions based on various EDP limits were assessed on probabilistic basis. To this end, fragility functions relating the likelihood of concrete cover spalling and bar buckling to various EDP limits were developed. The following main conclusions were reached:

(1) Drift ratio predictions at concrete cover spalling and bar buckling based on the two proposed expressions, Eqs. 8 and 9, respectively, were more accurate than those obtained based on other similar expressions found in the literature.

(2) Concrete compressive strain limits ranging from 0.004 to 0.007 resulted in drift ratio predictions at concrete cover spalling with comparable accuracy. Lower limits, however, are undesirable within the context of PBD since they may result in significantly low drift ratio capacities which would be challenging to design for, particularly in high seismic regions.

(3) Among the variable rebar tensile strain limits considered in this study, those established based on the proposed expression, Eq. 12, yielded the most accurate predictions of drift ratios at bar buckling. Constant rebar tensile strain limits ranging from 0.05 to 0.06 were found to have comparable accuracy in predicting drift ratios at bar buckling.

ACKNOWLEDGMENT

The financial contributions of the Green Construction Research & Training Center (GCRTC) at the University of British Columbia (UBC) and the Natural Sciences and Engineering Research Council of Canada (NSERC) were critical to conduct this research and are gratefully acknowledged.

REFERENCES

[1] SEAOC. (1995). *Vision 2000: performance based seismic engineering of buildings*. Sacramento, CA: Structural Engineers Association of California.

[2] Hose, Y., Silva, P., & Seible, F. (2000). “Development of a performance evaluation database for concrete bridge components and systems under simulated seismic loads.” *Earthquake Spectra*, 16(2), 413-442.

[3] Kowalsky, M. J. (2000). “Deformation limit states for circular reinforced concrete bridge columns.” *Journal of Structural Engineering*, 126(8), 869-878.

[4] Berry, M. and Eberhard, M. (2003). *Performance models for flexural damage in reinforced concrete columns*. PEER Report 2003/18. Berkeley, CA: Pacific Earthquake Engineering Research Center.

[5] Berry, M., M. Parrish, and M. Eberhard. 2004. PEER structural performance database, user’s manual. Berkeley, CA: Pacific Earthquake Engineering Research Center, Univ. of California

[6] Lehman, D., and Moehle, J. (2000). *Seismic performance of well-confined bridge columns*. PEER Report No. 1998/01. Berkeley, CA: Pacific Earthquake Engineering Research Center.

[7] Goodnight, J. C., Kowalsky, M. J., and Nau, J. M. (2016). “Strain limit states for circular RC bridge columns.” *Earthquake Spectra*, 32(3), 1627-1652.

[8] Murphy, T. P., Marsh, L., Bennion, S., Buckle, I. G., Nicolas, L., Anderson, D., Kowalsky, M., and Restrepo, J. 2020. *Proposed AASHTO guidelines for performance-based seismic bridge design*. NCHRP Research Report 949. Washington, DC: TRB.

[9] Marsh, M. L. and Stringer, S. J. (2013). *Performance-based seismic bridge design, a synthesis of highway practice*. NCHRP Synthesis-440. Washington, DC: TRB.

[10] Lehman, D., Moehle, J., Mahin, S., Calderone, A., and Henry, L. (2004). "Experimental evaluation of the seismic performance of reinforced concrete bridge columns." *Journal of Structural Engineering*, 130(6), 869-879.

[11] Salehi, M., Sideris, P., and Liel, A. B. (2020). "Assessing damage and collapse capacity of reinforced concrete structures using the gradient inelastic beam element formulation." *Engineering Structures*, 225, 111290.

[12] Priestley, M. J. N., Seible, F., and Calvi, G. M. (1996). *Seismic design and retrofit of bridges*. New York: Wiley.

[13] Scott, B. D., Park, R., and Priestly, M. N. (1982). ''Stress-strain behavior of concrete confined by overlapping hoops at low and high strain rates.'' *ACI Struct. J.*, 79(1), 13–27.

[14] Popovics, S. (1973). "A numerical approach to the complete stress strain curve for concrete." Cement and Concrete Research, 3(5), 583-599.

[15] Filippou F.C., Popov, E.P., and Bertero, V.V. (1983). *Effects of Bond Deterioration on Hysteretic Behavior of Reinforced Concrete Joints*. Report EERC 83-19. Earthquake Engineering Research Center, University of California, Berkeley.

[16] Mander J.B., Priestley M.J.N., and Park R. (1988). "Theoretical Stress-Strain Model for Confined Concrete." *Journal of Structural Engineering*, 114(8), 1804-1826.

[17] Karsan, I. D., and Jirsa, J. O. (1969). "Behavior of concrete under compressive loading." *Journal of Structural Division ASCE*, 95(ST12), 2543-2563.

[18] Zhao, J., and S. Sritharan. (2007). "Modeling of strain penetration effects in fiber-based analysis of reinforced concrete structures." *ACI Structural Journal*, 104(2), 133-141.

[19] Goodnight, J. C., Feng, Y., Kowalsky, M., and Nau, J. M. (2015). *The effects of load history and design variables on performance limit states of circular bridge columns - volume 2: experimental observations*. Juneau, AK: Alaska Department of Transportation & Public Facilities.

[20] Aldabagh, S., Hossain, F. and Alam, M. S. (2021). "Simplified predictive expressions of drift limit states for reinforced concrete circular bridge columns." *Journal of Structural Engineering*, ASCE, 148(3), 04021285.

[21] CSA (Canadian Standards Association). 2019. *Canadian highway bridge design code*. CSA S6-19. 12th ed. Rexdale, ON: CSA.